Cluster Monte Carlo study of multi-component fluids of the Stillinger-Helfand and Widom-Rowlinson type

Rongfeng Sun† and Harvey Gould

Department of Physics, Clark University, Worcester, MA 01610-1477

J. Machta

Department of Physics and Astronomy, University of Massachusetts, Amherst, MA 01003-3720

L. W. Chayes

Department of Mathematics, University of California, Los Angeles, CA 90095-1555

Abstract

Phase transitions of fluid mixtures of the type introduced by Stillinger and Helfand are studied using a continuum version of the invaded cluster algorithm. Particles of the same species do not interact, but particles of different types interact with each other via a repulsive potential. Examples of interactions include the Gaussian molecule potential and a repulsive step potential. Accurate values of the critical density, fugacity and magnetic exponent are found in two and three dimensions for the two-species model. The effect of varying the number of species and of introducing quenched impurities is also investigated. In all the cases studied, mixtures of q-species are found to have properties similar to q-state Potts models.

I. INTRODUCTION

Several years ago Stillinger and Helfand [1,2] introduced a simple but nontrivial model of fluid demixing. Their original model consists of a binary mixture of A and B particles. Particles of the same type do not interact with one another, but A and B particles interact with a repulsive potential such that the Mayer f-function is a Gaussian. This choice for the AB potential, known as the Gaussian molecule potential, greatly simplifies the calculation of virial coefficients and most work for this potential has been done using series methods [3,4]. The main motivation for this work is to confirm Ising universality for the critical exponents of continuum systems.

In this paper we study the Stillinger-Helfand model and some of its generalizations using cluster Monte Carlo methods. Where possible, we compare our results to the series analyses and to results for the Ising-Potts universality classes. Although the Gaussian molecule potential yields a more tractable virial expansion, it is easier to implement a cluster algorithm for the repulsive step potential. We also consider a generalization of the Stillinger-Helfand model to q species (components), such that particles of the same species do not interact but particles of different species interact with a repulsive potential. We expect that this generalization will be in the same universality class as the q-state Potts model for q not too large and another motivation for this study is to confirm this correspondence. For example, we know that the two-dimensional (2D) Potts model for $q > 4$ has a first-order transition. Does the q-component 2D Stillinger-Helfand model also have a first-order transition for $q > 4$? In addition, we consider the effect of quenched disorder by randomly adding fixed scattering centers. There are general arguments [5] that quenched disorder causes first-order transitions to become continuous. These arguments hold rigorously for 2D Potts models [6], but have not been studied for continuum models.

In previous work [7] cluster Monte Carlo methods were applied to the Widom-Rowlinson model [8]. The Widom-Rowlinson and Stillinger-Helfand models are closely related, the only difference is that the Widom-Rowlinson model has a hard-core interaction between different

species. In this paper, the invaded cluster Monte Carlo method introduced in Ref. [7] is extended to soft-core repulsive potentials and is used to find the phase transition point for a given temperature without prior knowledge of the critical fugacity. The invaded cluster method has almost no critical slowing for the Widom-Rowlinson model, and we find that similar results hold for the Stillinger-Helfand models studied here.

II. DESCRIPTION OF THE MODELS AND NOTATION

We consider q-component ($q \geq 1$) fluids in d dimensions with $d = 2, 3$. The components (species) have no self-interaction but particles of one species interact with particles of all other species via an isotropic repulsive potential, $U(r)$. We consider two choices for $U(r)$,

$$U_{\rm step}(r) = \begin{cases} U_0, & \text{if } r < \sigma \\ 0, & \text{if } r \geq \sigma \ , \end{cases} \tag{2.1a}$$

$$U_{\rm gm}(r) = -kT \ln(1 - e^{-r^2/\sigma^2}). \tag{2.1b}$$

The limit $\beta = 1/kT \to \infty$ for the step potential corresponds to the Widom-Rowlinson model. For the Gaussian molecule potential, the temperature T plays no role because the Boltzmann factor, $e^{-\beta U_{\rm gm}(r)} = 1 - e^{-r^2/\sigma^2}$ is, by design, independent of T.

In general, each component of the q-component fluid may have a distinct fugacity; however symmetry considerations dictate that a demixing transition occurs with all fugacities equal, and hence we set all the fugacities equal to a single value, z. For sufficiently small z, the q species are mixed, while for large z, there are q distinct phases because different species repel one another, with each phase predominately composed of one species. If q is not too large, there is expected to be a single demixing transition separating these regimes that is in the same universality class as the q-state Potts model.

For very large q, the correspondence between Potts models and Widom-Rowlinson models must break down. Although Potts models have a single ordering transition, Widom-Rowlinson models can be presumed to have an intermediate crystalline phase for $d \geq 3$ and

large q. To understand this phase, consider the limits $z \ll 1$ and $q \gg 1$, with the product $\lambda = qz$ order unity. Then non-overlapping particles appear with an effective fugacity of λ. However when two particles overlap, the cost is an additional factor of $1/q$ because the overlapping particles must be of the same species. Hence the limiting model is precisely the hard sphere gas which we presume has a crystalline phase in $d \geq 3$ [9]. It is therefore reasonable to assume that such a phase occurs in the Widom-Rowlinson models for large q and z of order q^{-1}. Needless to say, for fixed q, when the fugacity is sufficiently large, the model will demix, and thus the crystalline phase is an intermediate phase. We also expect an intermediate crystalline phase for large q soft-core Stillinger-Helfand models based on a mapping to a single component fluid with a repulsive soft-core potential. For example, the Gaussian core model [10] is known to crystallize in $d = 3$. Although intermediate phases do not occur for the usual Potts models, they are not a consequence of the continuum; indeed such phases are known to occur on the lattice for the site-dilute (annealed) Potts models [11] as well as for the lattice version of the Widom-Rowlinson model [12].

III. CLUSTER ALGORITHM

The algorithms used here are, broadly speaking, examples of cluster algorithms of the type first introduced by Swendsen and Wang [13,14]. Cluster algorithms have been found to be much more efficient than local algorithms such as the Metropolis algorithm for simulating spin systems and lattice gases near critical points. Cluster algorithms would be very useful for off-lattice systems, but no general cluster method has yet been developed; indeed, the *only* off-lattice models for which highly efficient cluster methods are known are models of the Stillinger-Helfand and Widom-Rowlinson type. The distinguishing features of this class of models are that particles of the same species have no self-interaction and that there is a purely repulsive interaction between particles of different species. In this case, graphical representations and clusters algorithms are available [15,16] and have been implemented for the Widom-Rowlinson model [7].

Cluster algorithms for spin systems work by identifying clusters of spins and then randomly flipping these clusters. Cluster are defined by placing bonds between nearest neighbor aligned spins with a probability that depends on the temperature. For fluid systems, bonds are placed between particles of the same type with a probability that depends on the temperature and the interaction potential. Instead of flipping spins, clusters of particles are removed from the system and then new particles are added via a nonuniform Poisson process that depends on the fugacity and the potential due to the remaining particles.

Cluster algorithms are typically used with fixed values of the external parameters such as temperature or fugacity. However, when the location of the phase transition is not known, much computational effort in studying the transition is spent in locating the transition. To avoid this problem, invaded cluster methods can be used [17,18] which automatically adjust a thermodynamic parameter (for example, temperature or fugacity) to its value at the phase transition. This adjustment is accomplished by using the fact (proved for the $q = 2$ case [15]) that the clusters just percolate at the transition. In invaded cluster algorithms, clusters are grown until a signature of percolation is observed. The value of the thermodynamic parameter at the transition is an output of the simulation obtained from the fraction of successful attempts to add particles or bonds to the system. The invaded cluster algorithm also may be used to distinguish first-order from continuous transitions as discussed in Ref. [18] for Potts models. This method for distinguishing the order of the transition is discussed below and will be used in Section IV C.

We first describe the cluster algorithm discussed in Section 3.5 of Ref. [15] for Stillinger-Helfand models and then discuss how it can be modified to be an invaded cluster algorithm. We assume that we have a configuration consisting of particle positions and a set of bonds connecting some of the particles and describe how to obtain the next configuration:

1. Identify all clusters of particles defined by the bonds. A particle with no bonds is considered to be a singleton cluster. For each cluster, independently and with probability $1/q$, label it a *black* cluster and with probability $1 - 1/q$ label it *white*.

2. Remove all particles in black clusters. The remaining white particles are at a set of positions W.

3. Replenish the black particles via a Poisson process with local intensity $y(x)$ given by

$$y(x) = ze^{-\beta V(x)}, \tag{3.1a}$$

$$V(x) = \sum_{y \in W} U(|x - y|). \tag{3.1b}$$

   where z is the fugacity and $U(r)$ the potential.

4. For each pair of black particles, place a new *bond* between them with probability $p(r)$ given by

$$p(r) = 1 - e^{-\beta U(r)}, \tag{3.2}$$

   where r is the separation between the particles. Note that $p(r)$ is minus the Mayer f-function for the potential.

5. Eliminate the white and black labels for the clusters.

This procedure comprises one Monte Carlo step.

Given a configuration of particle positions and bonds without species labels, it is possible to obtain a full multicomponent configuration where each particle has a species label. This assignment is accomplished by identifying clusters and then randomly and independently assigning one of the q species labels to each cluster. The species label of each particle is taken to be the species label of its cluster. This labeling of particles is only possible if q is a positive integer. However, the algorithm makes sense for all $q \geq 1$, in analogy to the relation between Potts models, which are defined for positive integer q, and random cluster models which interpolate between them and are defined for all $q > 1$.

It is instructive to consider the nature of the cluster configurations generated by the algorithm as a function of the fugacity for a fixed temperature. Suppose that the fugacity

and, hence, the density is very small. Then $p(r)$ is typically small because the particles are far apart, and most clusters are singletons. In step 2, a fraction $1/q$ of the particles is removed. In step 3, particles are replenished as a nearly ideal gas because the exponential factor in Eq. (3.1a) is a small perturbation except in the vicinity of the remaining particles. The end result is a nearly ideal multi-component gas. In the limit of large fugacity and density, we expect a phase in which a single species is predominant with a small admixture of the other species. The bonds connecting particles of the dominant species are sufficiently dense that almost all members of this species are in a single large cluster. The minority species are almost all in widely scattered singleton clusters. When the majority species is white, as occurs in about $1/q$ of the Monte Carlo steps, the large cluster is removed and then replaced as a nearly ideal gas in a slightly perturbed background potential generated by the minority species. An important feature of this picture is that the clusters do not percolate at small fugacity and do percolate at large fugacity. At some intermediate value of the fugacity, there must be a percolation transition. As discussed in Refs. [15,19,20], the percolation transition of the clusters coincides with the demixing transition of the fluid.

The coincidence of the percolation transition and the demixing transition justifies an invaded cluster version of the above cluster algorithm. The invaded cluster algorithm is very similar to the fixed z cluster algorithm described above except that steps 3 and 4 are modified as follows. Instead of putting down new black particles as a Poisson process at a fixed intensity, black particles are added to the system one at a time according to the potential $V(x)$ (see below). After each black particle is added, bonds between the new particle and all previously placed black particles are put down with probability $p(r) = 1 - \exp(-\beta U(r))$. The black clusters defined by these bonds are monitored after each particle is added, and the process of adding particles is stopped when a *stopping condition* is satisfied. For simulating the phase transition, the stopping condition is that one cluster *spans* the system. For periodic boundary conditions, spanning is taken to mean that a cluster wraps around the system in at least one of the d directions. The spanning condition insures that the algorithm simulates the phase transition [18].

In practice, a particle is added to the system according to the potential $V(x)$ by the following procedure. A particle is tentatively placed at a random position x. A random number r is chosen in the interval $[0, 1)$, and the particle placement is accepted if

$$r < e^{-\beta V(x)}; \tag{3.3}$$

otherwise the particle is rejected and another attempt is made to place a particle. Let $\tilde{z} = \langle N_{\rm tot}/L^d \rangle$, where $N_{\rm tot}$ is the total number of attempted particle placements in a Monte Carlo step, including both accepted and rejected placements, L^d is the system volume, and the brackets $\langle \ldots \rangle$ indicate an average over the simulation. Because the intensity $y(x)$, defined in Eq. (3.1a), and the Boltzmann factor $e^{-\beta V(x)}$ governing particle placements differ by a factor of the fugacity, we conclude that $\tilde{z}$ is an estimator of z_c, the value of the fugacity at the transition. Note that if the fluctuations $\sigma_{\tilde{z}}$ in $N_{\rm tot}/L^d$ are small, then the invaded cluster algorithm is essentially identical to the fixed fugacity algorithm operating at $z = z_c$. This identification justifies the use of the invaded cluster method. A more complete discussion of the invaded cluster method and the use of $\tilde{z}$ as an estimator of a critical parameter is given in Ref. [18].

Whenever the invaded cluster method simulates a system at its critical point, scaling methods can be used to obtain critical exponents from the size dependence of divergent thermodynamic quantities such as the compressibility or the susceptibility. To study the latter, we consider the quantity

$$\chi \equiv \frac{1}{L^d} \langle \sum_i s_i^2 \rangle \tag{3.4}$$

where s_i is the number of particles in the ith cluster. We now show that χ is related to the usual susceptibility. Consider, for simplicity, the discretized version of the Stillinger-Helfand model on a lattice of linear dimension L with spacing ϵ so that the total number of sites is $[L/\epsilon]^d$. The demixing order parameter at site x is given by $\delta\rho_1(x) \equiv n_1(x) - n(x)/q$, where $n_1(x) = 1$ if there is a particle of type 1 at site x and $n_1(x) = 0$ otherwise; $n(x)$ counts the presence of a particle of *any* type. The relevant susceptibility $\tilde{\chi}$ is defined by the second derivative of the pressure with respect to the (ordering) chemical potential:

$$\tilde{\chi} = \frac{1}{L^d} \sum_{x,y} \langle \delta\rho_1(x) \delta\rho_1(y) \rangle. \tag{3.5}$$

(The reason that ϵ does not enter explicitly into Eq. (3.5) is that the derivatives are with respect to the log of the activity and it is the activity that is scaled by ϵ.) For a given particle and bond configuration, averaging over assignments of species labels, it is clear that $\delta\rho_1(x)\delta\rho_1(y)$ vanishes unless the sites x and y are both occupied and in the same cluster, in which case the result is $q^{-2}(q-1)$. Thus, for a fixed particle-bond configuration, we obtain the number of particles in the cluster at x if we sum over y. Summing over x yields the sum of the squares of the cluster sizes so that $\tilde{\chi} = q^{-2}(q-1)\chi$, and hence we conclude that χ is related to the usual susceptibility. Finally, finite size scaling predicts that

$$\chi \sim L^{\gamma/\nu}, \tag{3.6}$$

so that the scaling of χ with system size can be used to extract the magnetic exponent γ.

Cluster methods also may be used to distinguish first-order from continuous transitions. For this purpose, a fixed density stopping rule is used. Black particles are added to the system until the density ρ reaches a fixed value and then $\tilde{z}$ is measured. In this way the canonical ensemble is simulated rather than the grand canonical ensemble. This procedure is done for a range of densities near the transition. If the transition is continuous, the fugacity is a strictly increasing function of ρ. However, if the transition is first-order, then the fugacity does not increase monotonically with increasing ρ in the coexistence region. Why does the nature of the $\tilde{z}$ versus ρ curve signify whether a transition is continuous or first-order? Suppose that the demixing transition of a q-component system is first-order. At the transition, there is coexistence of $q+1$ phases; q demixed phases and one mixed phase. Because the repulsive interaction is reduced for the demixed phases, these phases have a higher density than the mixed phase. Thus, in the thermodynamic limit, there is a range of ρ for which the fugacity is constant. Let ρ_1 be the density of the mixed phase and ρ_2 the density of the demixed phase. Because $\ln z = \partial s/\partial\rho$, where s is the entropy density, we have that s is a linear function of ρ in the coexistence region. More specifically, $s(\rho)$ is a linear

combination of $s(\rho_1)$ and $s(\rho_2)$, the entropy densities of the mixed and demixed phases. The linearity of $s(\rho)$ applies in the thermodynamic limit. However, for a finite system, the entropy density is not linear in the coexistence region. Consider a system with linear dimension L and periodic boundary conditions at density ρ. This system also can be viewed as an infinite system with periodic constraints on the particles. Let $s(\rho, L)$ be the entropy density of this periodically constrained system. Now suppose the constraints are removed and the system comes to equilibrium. If $\rho_1 \leq \rho \leq \rho_2$, demixing will occur spontaneously so that $s(\rho, L) \geq s(\rho)$ with the equality holding only at the endpoints of the coexistence range. Because $\ln z = \partial s/\partial \rho$, we must have that z is non-monotone in the coexistence region. This approach for distinguishing the order of a transition is very similar to the microcanonical Monte Carlo method used in Ref. [21].

IV. RESULTS

In Section IV A we present results for the 2D and 3D Stillinger-Helfand Gaussian molecule models. The two-component step potential model is discussed in Section IV B and the q-component step potential is discussed in Section IV C.

A. Gaussian molecule model in two and three dimensions

We simulated the Gaussian molecule model (with the potential $U_{\rm gm}$ defined in Eq. (2.1b)) using the invaded cluster method and the spanning rule described in Section III for a range of linear dimensions L up to 140 in $d = 2$ and 40 in $d = 3$. We choose units such that distances are measured in units of σ. We collected statistics for the number of particles in the spanning cluster M, the critical density ρ, the susceptibility χ, the estimator of the critical fugacity $\tilde{z}$ and its standard deviation $\sigma_{\tilde{z}}$, and the normalized autocorrelation function for the spanning cluster size, Γ_M. For each value of L we averaged over 10^5 Monte Carlo steps. The estimator of the critical density is the average number of particles (of any species) per unit area (volume) when the spanning condition is fulfilled. Although $U_{\rm gm}(r)$ does not

go to zero at finite r, it becomes very small for larger r and to speed the calculation, we set $U_{\rm gm}(r) = 0$ for $r \geq 3$.

Tables I and II show the L dependence of M, ρ, χ, $\tilde{z}$, $\sigma_{\tilde{z}}$, and τ_M for the 2D and 3D Stillinger-Helfand models, respectively. The integrated autocorrelation time τ_M is defined by

$$\tau_M = \frac{1}{2} + \sum_{t=1}^{\infty} \Gamma_M(t). \tag{4.1}$$

This time is approximately the number of Monte Carlo steps between statistically independent configurations and enters into the error estimate for M. In practice, $\Gamma_M(t)$ becomes indistinguishable from the noise for $t \approx 10$ Monte Carlo steps, and it is necessary to cut off the upper limit of the sum defining τ_M when the magnitude of Γ_M becomes comparable to its error.

Note that the fluctuations $\sigma_{\tilde{z}}$ in $\tilde{z}$ decrease with increasing L and that τ_M is small and hardly increases with L. These results demonstrate the validity and efficiency of the invaded cluster algorithm. The decrease in $\sigma_{\tilde{z}}$ shows that as L increases, the invaded cluster becomes essentially equivalent to a fixed parameter cluster algorithm for which detailed balance can be proven.

The error estimates for all quantities in Tables I and II except τ_M were obtained by computing the standard deviation of the quantity of interest and dividing by the square root of the number of measurements. This error estimate does not take into account correlations between successive Monte Carlo steps. To account for correlations, the error estimates in the tables for an observable O must be multiplied by $\sqrt{2\tau_O}$, where τ_O is the integrated autocorrelation time for O. The statistical errors for quantities derived from fits such as ρ_c and γ/ν include the factor $\sqrt{2\tau}$ except that τ_O is replaced by τ_M.

Figure 1 shows the results for $\rho(L)$ versus $1/L$ for the 2D Stillinger-Helfand model. The value of ρ in the limit of $L \to \infty$ is extrapolated from the finite size data by doing a linear least squares fit omitting the values for $L = 20$ and 40 yielding the result, $\rho_c(2) = 1.1644 \pm 0.0004$. A similar extrapolation for the critical fugacity yields $z_c(2) = 1.3536 \pm 0.0008$.

Similarly, extrapolating the result for the 3D Stillinger-Helfand model using the data for all available L yields $\rho_c(3) = 0.440 \pm 0.001$ and $z_c(3) = 0.5826 \pm 0.0013$. Our error values for these critical parameters are one standard deviation from the linear least squares fit of the fugacity or density versus $1/L$; no effort has been made to estimate systematic errors. All of the fits have acceptable goodness-of-fit probability values Q.

Our 3D value for the critical density is consistent with the series result of Lai and Fisher [4], $\rho_c(3) = 0.441 \pm 0.001$ (Eq. (36) of Ref. [4]) but our critical fugacity is somewhat larger than their value, $z_c(3) = 0.5785 \pm 0.0002$ (Eq. (44) of Ref. [4]). Note that Lai and Fisher report results using a different convention so that their values of ρ_c and z_c must be divided by $\pi^{d/2}$ to compare with our values.

The exponent ratio γ/ν can be obtained from the scaling of the susceptibility χ with L according to Eq. (3.6). Figure 2 shows a log-log plot of χ versus L for the 2D Gaussian molecule model. A least squares fit of all the data to a simple power law does not yield an acceptable goodness of fit value Q. If the smallest value of L is omitted, we obtain $\gamma/\nu = 1.745 \pm 0.001$ with $\chi^2 = 6.2$, $Q = 0.19$, and DF = 4 (degrees of freedom). The Q value indicates a reasonable fit to a simple power law, but the fitted value of γ/ν is $5\,\sigma$ from the 2D Ising value of $\gamma/\nu = 7/4$. A reasonable explanation of this result is that the 2D Gaussian molecule is, indeed, in the 2D Ising universality class, but that there are relatively slowly varying corrections to scaling.

A least squares fit to all the data for the susceptibility χ for the 3D Gaussian molecule model yields $\gamma/\nu = 1.9626 \pm 0.0044$ with $\chi^2 = 0.11$, DF = 2, and $Q = 0.95$. The Q value near unity suggests that the data is well fit to a pure power law. Recent high precision Monte Carlo studies of the 3D Ising model [22] yield $\gamma/\nu = 1.9630(30)$ which is consistent with our results. Our results add weight to the hypothesis that the Stillinger-Helfand model is in the Ising universality class for both 2D and 3D. The relatively high precision results for γ/ν from the Gaussian molecule model suggests that models of the Stillinger-Helfand type may be useful for high precision studies of the 3D Ising universality class. The isotropy of the interaction and absence of an underlying lattice might make for smaller corrections to

scaling in Stillinger-Helfand models compared to lattice spin models.

B. Step potential in 2D

Table III summarizes our results for the 2D Stillinger-Helfand model with the step potential given by Eq. (2.1a) and temperature $T = 1$ (measured in units of U_0). For each value of L we averaged over 10^6 Monte Carlo steps. The results are qualitatively similar to the Gaussian molecule model. Table IV shows the temperature dependence of the measured quantities for L fixed at $L = 20$. The values of ρ and $\tilde{z}$ at low temperatures should reduce to the Widom-Rowlinson model. In Ref. [7] we measured the critical parameters of the Widom-Rowlinson model using the invaded cluster method. For $L = 40$ (the smallest size measured) we obtained $\rho = 1.525$ and $\tilde{z} = 1.720$, values that are close to the values of ρ and $\tilde{z}$ for the two lowest temperatures in Table IV. This agreement confirms that the step potential is continuously connected to the hard core potential.

If the $L = 20$ data point is omitted, we obtain from a least squares fit to the data for the susceptibility χ, $\gamma/\nu = 1.7434 \pm 0.0009$ with $\chi^2 = 0.52$, $Q = 0.81$, and DF $= 3$.

C. Dependence of the order of the transition on q and on impurities

The critical properties of the q-component Stillinger-Helfand model are expected to be closely related to the q-state Potts model. One of the features of the q-state Potts model is that the transition is continuous for small q and is first-order for $q > q_c(d)$, where $q_c(2) = 4$ and $2 < q_c(3) < 3$. We have used the method described in Section III to determine the order of the transition as a function of q for the q-component Stillinger-Helfand step potential model. Figure 3 shows the fugacity $\tilde{z}$ as a function of ρ for $d = 2$ for $L = 40$ and $T = 1$. Note that for $q = 3$ the curve is clearly monotonically increasing, which implies a continuous transition. For $q \geq 5$ the curves are clearly non-monotonic, which implies a first-order transition. For $q = 4$ the curve is essentially flat within the error bars (whose size is approximately that of the symbols). Although the effective value of q_c is expected

to vary with L, these results are consistent with the hypothesis that $q_c(2) = 4$ for the 2D Stillinger-Helfand step potential model.

Figure 4 shows $\tilde{z}$ as a function of ρ for the 3D Stillinger-Helfand step potential model for $L = 20$ and $T = 1$. The $q = 2$ curve is clearly monotonically increasing while the $q = 3$ is clearly not, implying that $2 < q_c(3) < 3$ as for the 3D Potts model.

Finally, we have studied the effect of quenched impurities on the nature of the transition for the $q = 3$ Stillinger-Helfand step potential model. The impurities consist of randomly placed scatterers that interact with all the fluid particles via the same repulsive step potential that exists between different components. Figure 5 shows a plot of $\tilde{z}$ versus ρ for the $q = 3$ Stillinger-Helfand step potential model in 3D for four impurity densities ranging from 0.025 to 0.0625. For each of the 10 impurity configurations considered for a given density, data from 10^3 Monte Carlo steps are collected. For the two lowest impurity concentrations, the $\tilde{z}$ versus ρ curve is non-monotonic as is the case for the pure system, while for the two highest impurity concentrations, the curve is monotonic indicating a crossover to a continuous transition. This behavior is in accord with general arguments [5] that the presence of quenched impurities should cause a first-order transition to become continuous. It is not clear from our data whether there is a critical value of the disorder below which the transition remains continuous or whether the crossover at finite disorder strength is a finite size effect and that any strength of disorder is sufficient to make the transition continuous in the thermodynamic limit.

V. DISCUSSION AND CONCLUSIONS

We have studied the Stillinger-Helfand model and several generalizations using the invaded cluster algorithm. Our results for q-component Stillinger-Helfand models with $2 \leq q \leq 8$ are consistent with the hypothesis that these models are in the same universality class as the corresponding Potts models. In addition, we have shown that the addition of quenched disorder causes the demixing transition to change from first-order to continous for those values of q for which the pure system transition is first-order. For the case $q = 2$

and $d = 2$, our results for the magnetic exponent are outside the statistical error bars of the exact Ising value. However, we believe that this difference is most likely the result of slowly varying corrections to scaling. It would be useful to consider larger system to confirm Ising universality. It would also be interesting to consider larger values of q to explore the possibility of an intermediate crystalline phase in Stillinger-Helfand models.

VI. ACKNOWLEDGEMENTS

This work was supported by NSF grants PHY-9801878 (RS), DMR-9633385 (HG), DMR-9978233 (JM), DMS-9971016 (LC), and NSA grant MDA904-98-1-0518 (LC). We thank Gregory Johnson for useful discussions.

†Present address: Courant Institute of Mathematical Sciences, 251 Mercer Street, New York, NY 10012.

REFERENCES

[1] F. H. Stillinger and E. Helfand, *J. Chem. Phys.* **41**, 2495 (1964).

[2] E. Helfand and F. H. Stillinger, *J. Chem. Phys.* **49**, 1232 (1968).

[3] A. Baram, M. W. Maddox, and J. S. Rowlinson, *Mol. Phys.* **76**, 1093 (1992).

[4] S.-N. Lai and M. E. Fisher, *Mol. Phys.* **88**, 1373 (1996).

[5] K. Hui and A. N. Berker, *Phys. Rev. Lett.* **62**, 2507 (1989); **63**, 2433 (E) (1989).

[6] M. Aizenman and J. Wehr, *Phys. Rev. Lett.* **62**, 2503 (1989).

[7] G. Johnson, H. Gould, J. Machta, and L. K. Chayes, *Phys. Rev. Lett.* **79**, 2612 (1997).

[8] B. Widom and J. S. Rowlinson, *J. Chem. Phys.* **52**, 1670 (1970).

[9] H. L. Frisch and J. K. Percus, Phys. Rev. E **60**, 2942 (1999).

[10] F. H. Stillinger and T. A. Weber, *J. Chem. Phys.* **68**, 3837 (1978).

[11] L. Chayes, R. Kotecký, and S. Shlosman, *Comm. Math. Phys.* **171**, 203 (1995).

[12] L. K. Runels and J. L. Lebowitz, *J. Math. Phys.* **15**, 1712 (1974).

[13] R. H. Swendsen and J. S. Wang, *Phys. Rev. Lett.* **58**, 86 (1987).

[14] M. E. J. Newman and G. T. Barkema, *Monte Carlo Methods in Statistical Physics*, (Oxford U. Press, Oxford, 1999).

[15] L. Chayes and J. Machta, *Physics* A **254**, 477 (1998).

[16] O. Haggstrom, M. N. M. Lieshout, and J. Moller, *Bernoulli* **5**, 641 (1999).

[17] J. Machta, Y. S. Choi, A. Lucke, T. Schweizer, and L. V. Chayes, *Phys. Rev. Lett.* **75**, 2792 (1995).

[18] J. Machta, Y. S. Choi, A. Lucke, T. Schweizer, and L. M. Chayes, *Phys. Rev.* E **54**, 1332 (1996).

[19] W. Klein, *Phys. Rev. B* **26**, 2677 (1982).

[20] J. T. Chayes, L. Chayes, and R. Kotecký, *Comm. Math. Phys.* **172**, 551 (1995).

[21] D. H. E. Gross, A. Ecker, X. Z. Zhang, *Annalen Phys.* **5**, 446 (1996).

[22] H. W. J. Blöte, E. Luijten, and J. R. Heringa, *J. Phys. A: Math. Gen.* **28**, 6289 (1995).

TABLE I. The L dependence of the number of particles in the spanning cluster M, the critical density ρ, the susceptibility χ, the estimator of the critical fugacity $\tilde{z}$, its standard deviation $\sigma_{\tilde{z}}$, and decorrelation time τ_M for the 2D Gaussian molecule potential. The averages are over 10^5 spanning clusters. The error estimates were obtained by computing the standard deviation of the quantity of interest and dividing by the square root of the number of measurements. The error estimates for τ_M are obtained from the variation of τ with the upper limit in the summation of Eq. (4.1) and hence represent an estimate of the systematic error. The autocorrelation function $\Gamma_M(t)$ is distinguishable from the noise for $t \sim 10$ Monte Carlo steps.

L	M	ρ	χ	$\tilde{z}$	$\sigma_{\tilde{z}}$	τ_M
20	297.1(1)	1.105(1)	245.2(5)	1.3286(8)	0.257	0.56(1)
40	1095(1)	1.1317(4)	832.5(10)	1.3469(6)	0.183	0.63(3)
60	2346(2)	1.1418(3)	1695(2)	1.3504(5)	0.149	0.68(3)
80	4017(4)	1.1472(3)	2796(2)	1.3516(5)	0.131	0.71(5)
100	6098(5)	1.1503(2)	4119(3)	1.3519(4)	0.117	0.75(3)
120	8587(7)	1.1532(2)	5670(3)	1.3524(4)	0.108	0.76(3)
140	11462(10)	1.1547(2)	7419(5)	1.3519(4)	0.0982	0.79(2)

TABLE II. The L dependence of M, ρ, χ, $\tilde{z}$, $\sigma_{\tilde{z}}$, and τ_M for the 3D Gaussian molecule potential. The averages are over 10^5 spanning clusters. The error estimates are calculated as discussed in the caption of Table I. represents one standard deviation. The autocorrelation function $\Gamma_M(t)$ is distinguishable from the noise for $t \sim 60$ Monte Carlo steps.

L	M	ρ	χ	$\tilde{z}$	$\sigma_{\tilde{z}}$	τ_M
10	171.6(3)	0.435(2)	35.7(2)	0.577(2)	0.103	0.52(4)
20	956(2)	0.438(1)	138.9(4)	0.580(1)	0.0582	0.55(3)
30	2614(3)	0.438(1)	308(1)	0.581(1)	0.0424	0.57(2)
40	5344(6)	0.439(1)	542(2)	0.581(1)	0.0341	0.58(3)

TABLE III. The L dependence of M, ρ, χ, $\tilde{z}$, $\sigma_{\tilde{z}}$ and τ_M for the 2D Stillinger-Helfand step potential model at $T = 1$. The averages are over 10^6 spanning clusters. The autocorrelation function $\Gamma_M(t)$ is distinguishable from the noise for $t \sim 10$ Monte Carlo steps.

L	M	ρ	χ	$\tilde{z}$	$\sigma_{\tilde{z}}$	τ_M
20	509.5(2)	1.9249(3)	720.7(5)	2.2626(4)	0.379	0.585(5)
40	1871.8(6)	1.9633(2)	2429(2)	2.2819(3)	0.270	0.665(10)
60	4001(2)	1.9779(3)	4927(3)	2.2856(4)	0.219	0.702(10)
80	6855(2)	1.9855(2)	8131(4)	2.2865(3)	0.191	0.737(10)
100	10411(3)	1.9902(1)	12000(6)	2.2864(2)	0.169	0.772(15)
120	14651(4)	1.9934(1)	16494(7)	2.2860(2)	0.154	0.783(10)

TABLE IV. The T dependence of M, ρ, χ, $\tilde{z}$, $\sigma_{\tilde{z}}$, and τ_M for the 2D Stillinger-Helfand step potential model at $L = 20$. The averages are over 10^6 MC steps. The autocorrelation function $\Gamma_M(t)$ is distinguishable from the noise for $t \sim 60$ Monte Carlo steps. The computational time required for a $L = 20$ system of $T = 10$ is approximately a week on a 533 MHz Alpha processor.

T	M	ρ	χ	$\tilde{z}$	$\sigma_{\tilde{z}}$	τ_M
0.05	411.1(2)	1.4905(3)	470.3(3)	1.7015(4)	0.310	0.58(0.5)
0.2	412.2(2)	1.4950(2)	472.4(3)	1.7072(4)	0.304	0.57(0.5)
0.5	439.1(2)	1.6076(2)	535.9(3)	1.8508(4)	0.326	0.58(0.5)
1	509.5(2)	1.9249(2)	720.6(4)	2.2626(4)	0.379	0.59(1)
3	763.0(3)	3.3065(4)	1612.7(8)	4.1052(6)	0.598	0.62(0.5)
5	963.1(7)	4.6606(4)	2567(2)	5.9353(8)	0.785	0.64(1)
7	1133(1)	5.9934(5)	3551(2)	7.7433(10)	0.957	0.65(1)
10	1353(1)	7.9680(9)	5059(4)	10.426(2)	1.182	0.66(1)

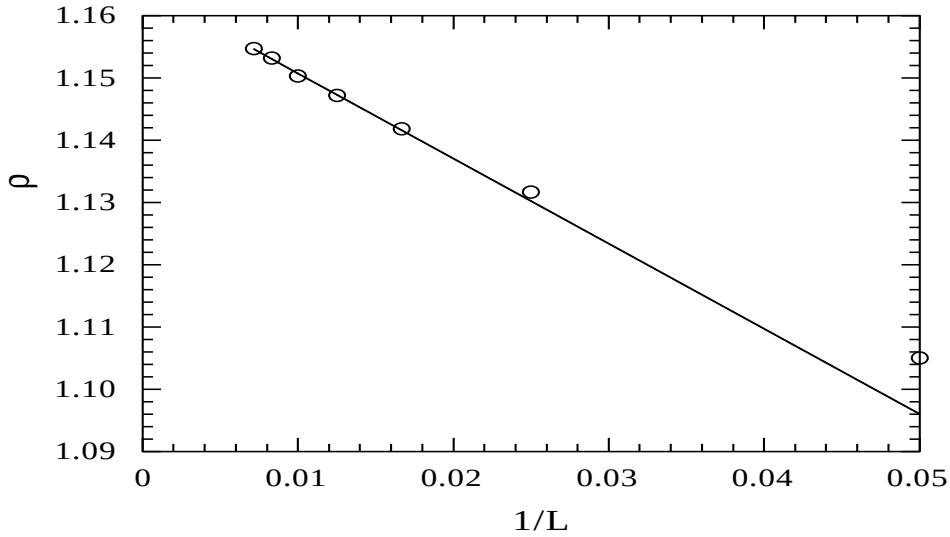

FIG. 1. Plot of ρ versus $1/L$ for the 2D Stillinger-Helfand Gaussian molecule model. The straight line represents a least squares fit omitting the value for $L = 20$ and 40. The extrapolated result is $\rho_c = 1.1644 \pm 0.0004$.

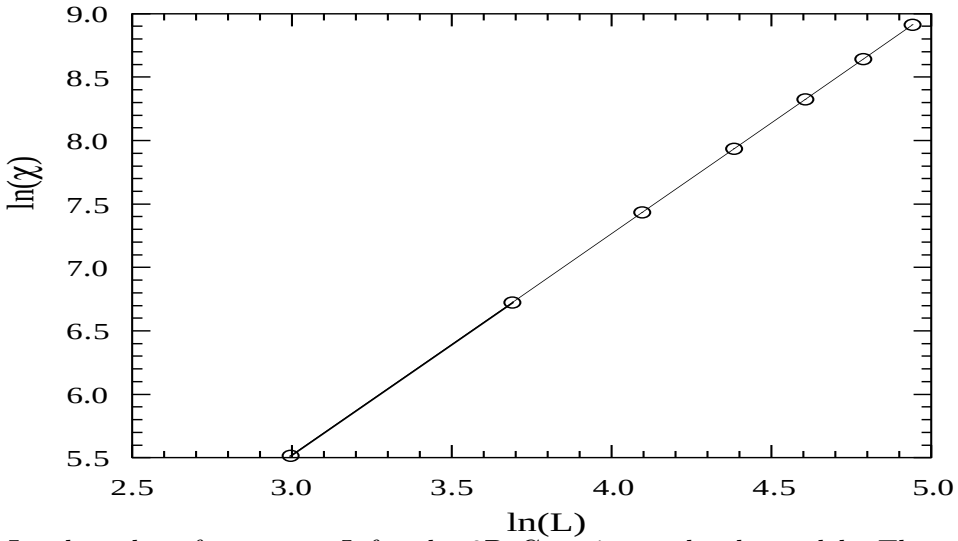

FIG. 2. Log-log plot of χ versus L for the 2D Gaussian molecule model. The straight line represents the best fit to the data, omitting $L = 20$, with $\gamma/\nu = 1.745$.

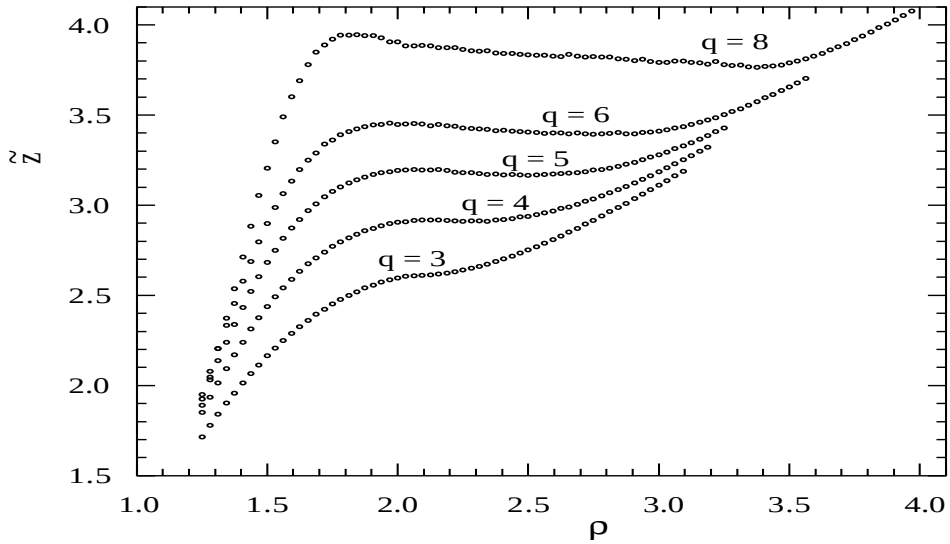

FIG. 3. Plot of the fugacity $\tilde{z}$ versus ρ for the 2D Stillinger-Helfand step potential model at $T = 1$, $L = 40$, for $q = 3, 4, 5, 6$, and 8. Each point is averaged over 20,000 MC steps. The error bars are of the size of the markers.

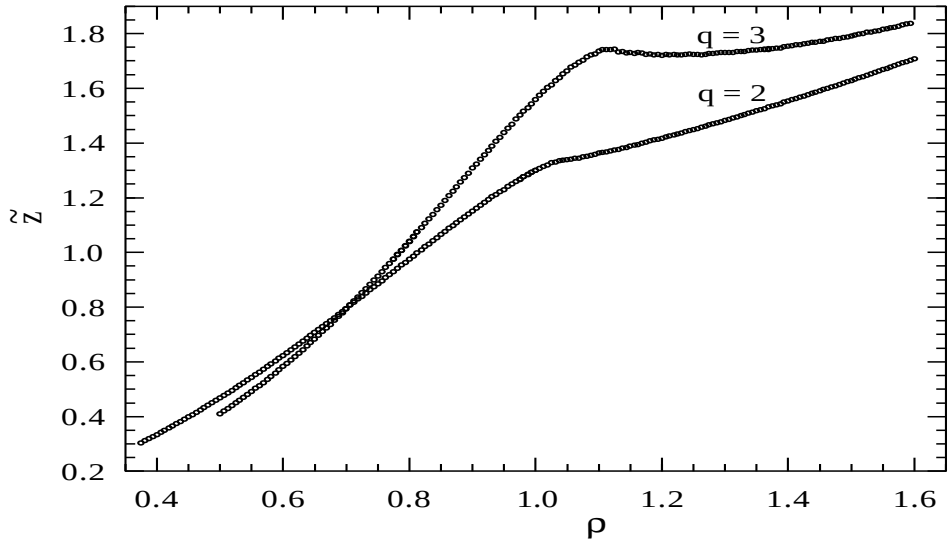

FIG. 4. Plot of $\tilde{z}$ versus ρ for the 3D WR step potential model at $T = 1$, $L = 20$, for $q = 2$ and 3. Each point is averaged over 1500 MC steps. The error bars are of the size of the markers.

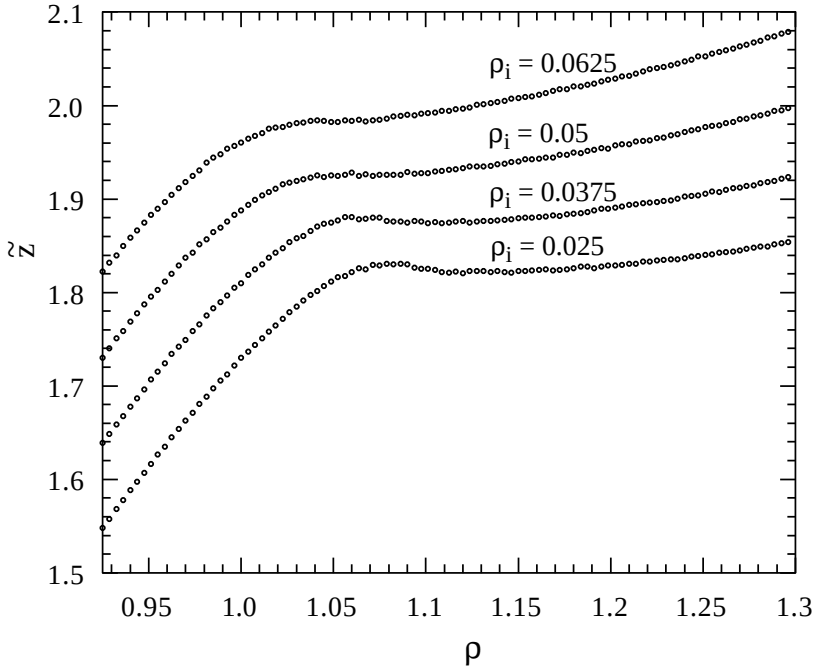

FIG. 5. Plot of $\tilde{z}$ versus ρ for the $q = 3$ Stillinger-Helfand step potential model in 3D with quenched impurities at $T = 1$ and $L = 20$. The 4 traces in the graph correspond to 200, 300, 400 and 500 fixed impurity particles, corresponding to impurity densities equal to 0.025, 0.0375, 0.05, and 0.0625.